Nanoscale

PAPER

View Article Online
View Journal | View Issue

Cite this: *Nanoscale*, 2019, **11**, 23035

Highly selective encapsulation and purification of U-based C_{78}-EMFs within a supramolecular nanocapsule†

Carles Fuertes-Espinosa,[a] Jesse Murillo,[b] Marco E. Soto,[b] Maira R. Ceron,[b] Roser Morales-Martínez,[c] Antonio Rodríguez-Fortea, [c] Josep M. Poblet, [c] Luis Echegoyen *[b] and Xavi Ribas *[a]

Received 4th September 2019,
Accepted 5th November 2019

DOI: 10.1039/c9nr07660c

rsc.li/nanoscale

The ability of the tetragonal prismatic nanocapsule **1**·$(BArF)_8$ to selectively encapsulate U-based C_{78} EMFs from a soot mixture is reported, showing enhanced affinity for C_{78}-based EMFs over C_{80}-based EMFs. Molecular recognition driven by the electrostatic interactions between the host and guest is at the basis of the high selectivity observed for ellipsoidal C_{78}-based EMFs compared to spherical C_{80}-based EMFs. In addition, DFT analysis points towards an enhanced breathing adaptability of nanocapsule **1**·$(BArF)_8$ to C_{78}-based EMFs to further explain the selectivity observed when the host is used in the solid phase.

Introduction

Since the discovery of fullerenes in 1985, tremendous interest has been devoted to exploit the cavity of carbon cages for hosting guest atoms or molecules. Specifically, endohedral metallofullerenes (EMFs) typically feature monoatomic or diatomic metal cations of the type $X@C_{2n}$, $X_2@C_{2n}$ (X = metal, and $60 \leq 2n \leq 88$), and also metal clusters such as trimetallic nitrides (M_3N), dimetallic carbides (M_2C and M_2C_2) and metallic oxides and sulphides (M_4O_2, M_2O, M_2S) have been described, among others.[1,2] Interest on these species is due to multiple reasons: (a) the intrinsic nature of the interaction of the naked cation(s) with the carbon cage,[3,4] (b) the unprecedented electronic and magnetic properties of the EMF due to the stabilization of otherwise non-existing clusters,[5] and (c) the cluster-dependent exohedral reactivity of the EMF.[6–11] However, the accumulation of practical amounts of EMFs to study their spectroscopy and their reactivity is hampered by three limiting factors: (1) the synthesis of soot with significant amounts of the desired EMF, (2) the lack of selectivity during their production, and (3) tedious and time-consuming HPLC chromatographic techniques to enrich or purify the selected EMF. Even more challenging is the chromatographic separation of EMFs with the same carbon cage and differing only in the nature of the cluster.[12] Alternative non-chromatographic approaches include the "stir and filter" method (SAFA) that consists of the immobilization of empty cyclopentadienyl- and amino-functionalized silica to enrich the soot with EMFs.[13,14] Also, the addition of Lewis acids such as $FeCl_3$, $AlCl_3$ or $TiCl_4$ allowed the separation of EMFs upon precipitation, while empty fullerenes remained in solution.[15] However, these methods are commonly used as a pre-enrichment of EMFs of a given soot and HPLC chromatography is ultimately necessary. On the other hand, Echegoyen reported the electrochemical purification of Sc_3N-based EMFs.[16]

Over the past years, scarce examples of the encapsulation of EMFs into supramolecular hosts have been reported, *i.e.* $Sc_3N@C_{80}$ or $Gd@C_{82}$.[17–19] Very recently, our group has developed the purification of EMFs by selective encapsulation in supramolecular nanocapsules. Following this strategy, we have recently reported the purification and isolation of $Sc_3N@C_{80}$ (I_h–D_{5h} mixture),[20] $U_2@I_h$-C_{80} and $Sc_2CU@I_h$-C_{80} from different soot.[21] In this work, we expand the ability of the tetragonal prismatic nanocapsule **1**·$(BArF)_8$ to selectively encapsulate novel U-based C_{78} EMFs, showing enhanced affinity for C_{78}-based EMFs compared to C_{80}-based EMFs (Fig. 1). The high selectivity observed is discussed based on the molecular recognition driven by the electrostatic interactions between the host and guest. In addition, the breathing ability of our receptor in the solid phase to better adapt to C_{78}-based EMFs is supported by DFT analysis.

[a]QBIS-CAT group, IQCC and Dept. Química, Universitat de Girona, Campus de Montilivi, E-17003 Girona, Catalonia, Spain. E-mail: xavi.ribas@udg.edu
[b]Department of Chemistry, University of Texas at El Paso, 500 West University Avenue, El Paso, Texas 79968, USA. E-mail: echegoyen@utep.edu
[c]Departament de Química Física i Inorgánica, Universitat Rovira i Virgili, C/Marcel·lí Domingo 1, 43007 Tarragona, Catalonia, Spain

†Electronic supplementary information (ESI) available: EMF soot preparation and experimental and computational details. See DOI: 10.1039/c9nr07660c

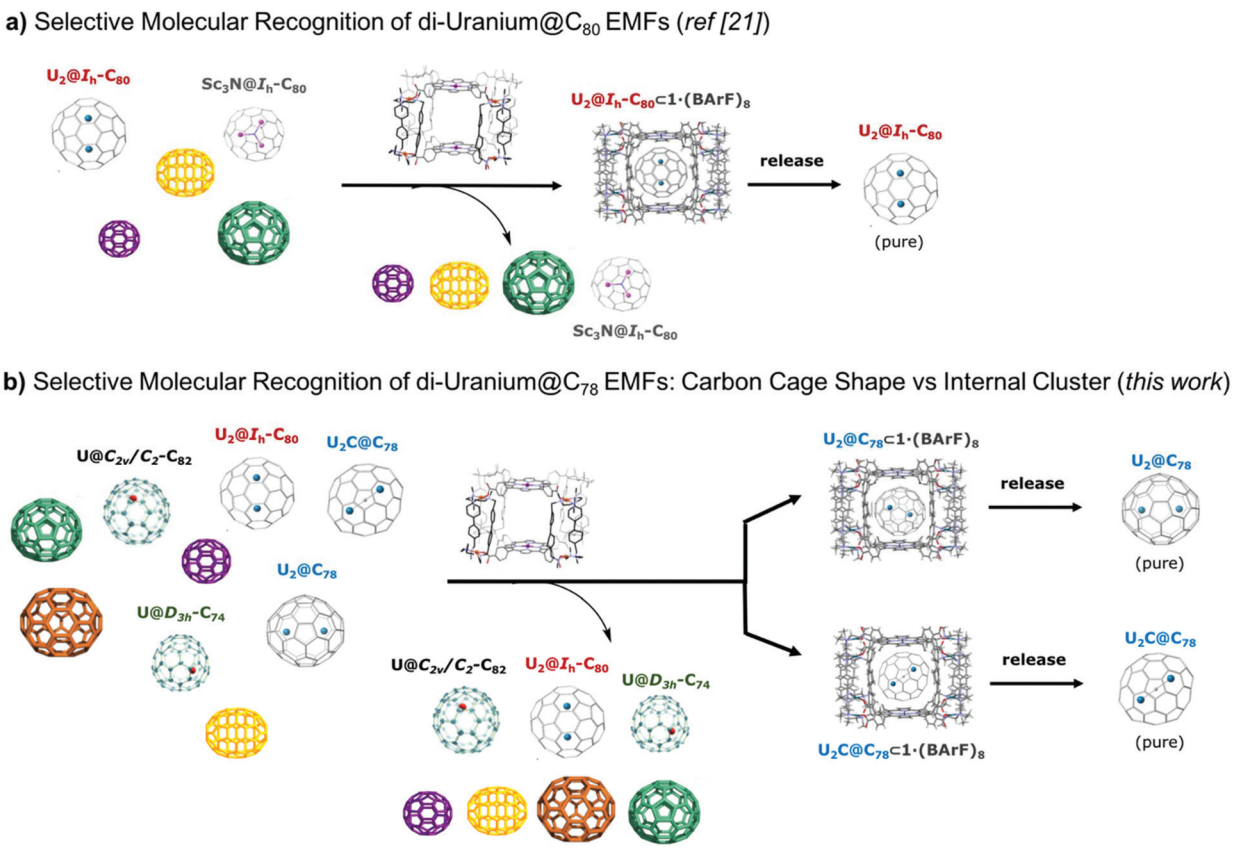

Fig. 1 (a) Non-chromatographic purification of U-based@C_{80} EMF by selective encapsulation in supramolecular nanocage **1a**·$(BArF)_8$. (b) Highly selective encapsulation and purification of U-based@C_{78} EMFs (this work).

Results and discussion

Previous investigations revealed that supramolecular nanocapsule **1**·$(BArF)_8$ is able to selectively recognize di-uranium-based C_{80} EMFs, in the presence of many other empty fullerenes and EMFs.[21] The production of a new family of uranium-based C_{78} EMFs allowed us to study the electronic and shape complementarity of **1**·$(BArF)_8$ towards these new compounds, in comparison to the previously described selectivity for uranium-based C_{80} EMFs. The low production yield and the complexity of the soot containing di-uranium-based C_{78} EMFs make their chromatographic separation extremely challenging. Aiming at the straightforward isolation of these new EMFs, crystals of **1**·$(BArF)_8$ were soaked in a toluene solution of the crude soot containing di-uranium-based C_{78} EMFs along with many empty fullerenes and mono-uranium EMFs with different size carbon cages. On monitoring the host–guest complexation by LDI-TOF analysis of the species remaining in solution, we clearly observed the selective and quantitative uptake of di-uranium-based C_{78} EMF species (U_2@C_{78} and U_2C@C_{78}) after 3 hours, observing a drastic decrease of the peaks belonging to these compounds (Fig. 2), attributed to the inclusion of the EMF within the cavity of solid **1**·$(BArF)_8$. Taking advantage of the encapsulation of the di-uranium@C_{78} EMFs in a crystalline material of the supramolecular nanocapsule, we isolated the solid (di-uranium@C_{78} EMFs)⊂**1**·$(BArF)_8$ complexes simply by filtration. Subsequently, the selectively trapped guests were easily released by washing the crystals with carbon disulfide, in analogy to our previously reported solvent-washing protocol (Fig. 2, bottom).[22] LDI-TOF analysis of the released guests confirms an exceptional selectivity towards U_2@C_{78} and U_2C@C_{78} compared to the rest of the compounds present in the starting soot, including U_2@C_{80}, which is known to show very high affinity for **1**·$(BArF)_8$. Remarkably, the target compounds were not kinetically trapped in the cage cavity and could be easily recovered by exploiting the orthogonal solubility between the host and the guest.

To better understand the effect of the size and the shape of the guests on the specific binding observed, we then explored the molecular recognition of U_2@C_{78} in the presence of a variety of U-based EMFs (U@C_{74}, U@C_{82} and U_2@C_{80}). The addition of crystalline **1**·$(BArF)_8$ to a toluene solution of the soot resulted in a clean and selective binding of U_2@C_{78} over the rest of the EMFs (Fig. 3). The trapped guest was successfully recovered and the LDI-TOF analysis of the released EMF evidenced the unique encapsulation of U_2@C_{78}. The presence of the same metal cluster in U_2@C_{78} and U_2@C_{80}, which transfers an equal number of electrons to the carbon cages,

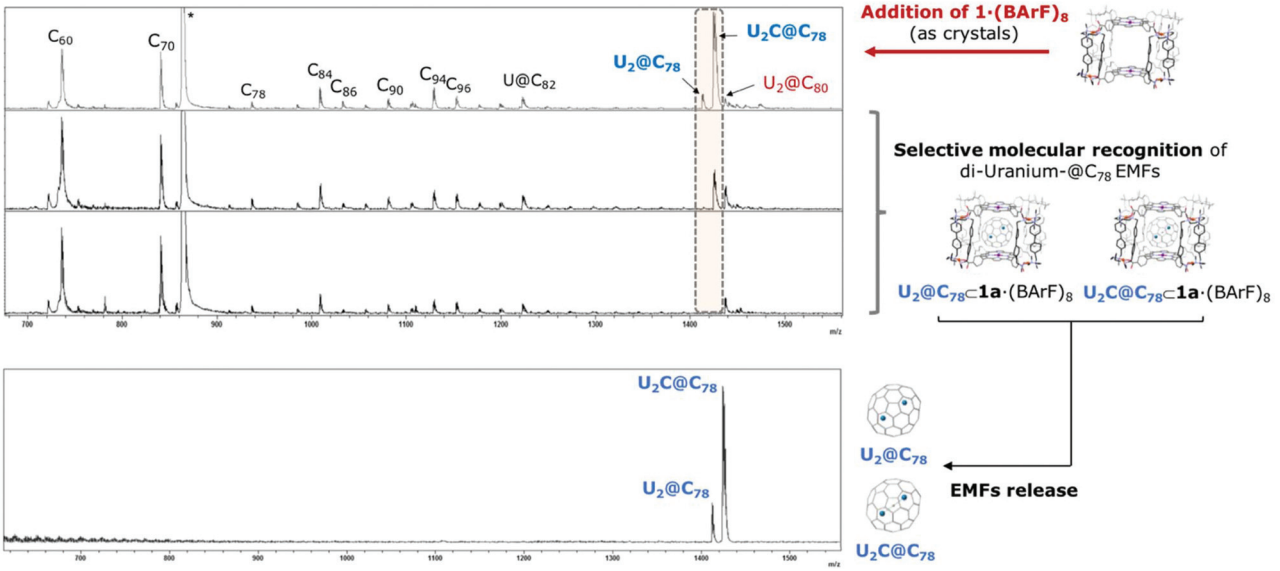

Fig. 2 LDI-TOF monitoring of the remaining supernatant over time during the selective encapsulation of $U_2@C_{78}$ and $U_2C@C_{78}$ within crystals of **1**·$(BArF)_8$ (top). Spectrum of released guests trapped during the molecular recognition (bottom).

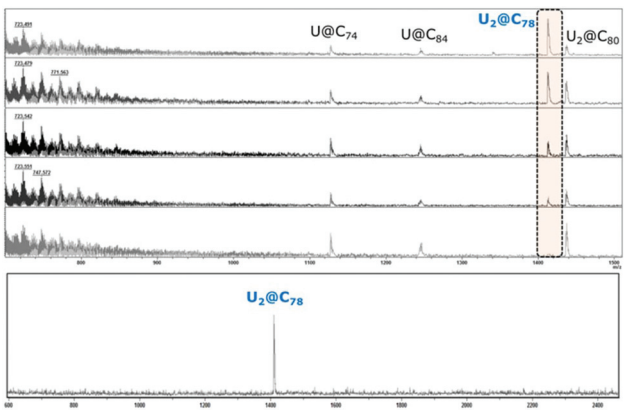

Fig. 3 LDI-TOF monitoring of the remaining supernatant over time during the selective molecular recognition of $U_2@C_{78}$ in a complex soot containing differently sized U-based EMFs (top). Spectrum of pure $U_2@C_{78}$ released from **1**·$(BArF)_8$ (bottom).

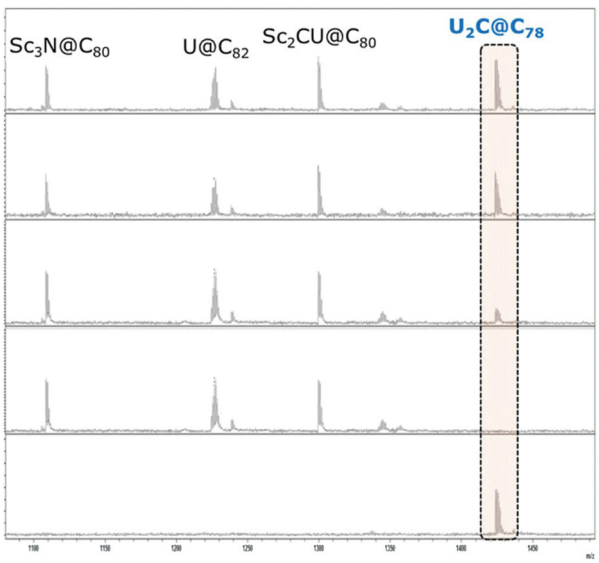

Fig. 4 LDI-TOF monitoring of the remaining supernatant over time during the selective molecular recognition of $U_2C@C_{78}$ in a soot containing C_{80}- and C_{82}-based EMF. Spectrum of pure $U_2C@C_{78}$ released from **1**·$(BArF)_8$ (bottom).

suggested that the selective molecular recognition events are governed by the size/shape relationship between the host and guest. The crystal structures of the previously reported D_{3h}-C_{78} and I_h-C_{80} EMFs showed very similar sizes of the carbon cages,[1] independent of the internal cluster hosted. Thus, the selectivity observed suggested enhanced π-interactions with the flattened regions of the ellipsoidal-shaped D_{3h}-C_{78} in comparison to the spherical I_h-C_{80} carbon cage.

Another soot containing U-based EMFs different from $U_2@C_{78}$ (with a similar proportion of $U_2C@C_{78}$, $Sc_2CU@C_{80}$, $U@C_{82}$ and $Sc_3N@C_{80}$) was studied to evaluate the importance of the carbon cage (size and shape) or the internal cluster (electrostatics) in the observed selectivity (Fig. 4). The selective encapsulation of $U_2C@C_{78}$ was observed upon the addition of crystalline **1**·$(BArF)_8$ to the corresponding soot solution in toluene; LDI-TOF analysis revealed a progressive decrease of the peak of $U_2C@C_{78}$ until its complete disappearance after 4.5 h (Fig. 4). LDI-TOF analysis of the released guest showed a single peak at m/z = 1424.0707, confirming the purification of $U_2C@C_{78}$. Remarkably, the ability of nanocapsule **1**·$(BArF)_8$ to preferentially encapsulate C_{78} over C_{80} EMFs was further evidenced by the encapsulation of $Sc_3N@C_{78}$ over $U_2@C_{80}$ (see Fig. S2†). Therefore, the shape of the carbon cage rules over

the nature of the internal cluster, with a higher affinity for C_{78}-based EMFs, irrespective of the nature of the internal cluster.

The presence of EMFs only differing in the nature of the internal clusters is very common in actinide-based EMF soot, making their chromatographic separation very challenging. We previously described the important role of the electron density distribution of EMFs only differing in the internal cluster ($U_2@I_h$-C_{80} *versus* $Sc_2CU@I_h$-C_{80} or $Sc_3N@I_h$-C_{80}) to allow their stepwise separation within nanocapsule $\mathbf{1}\cdot(BArF)_8$.[21] We hypothesize that the differences in the cluster arrangement of $U_2@C_{78}$ and $U_2C@C_{78}$ could promote different electronic distributions that could impact the electrostatic interaction with $\mathbf{1}\cdot(BArF)_8$. Therefore, we added precise amounts of crystalline materials of $\mathbf{1}\cdot(BArF)_8$ to a sample mainly containing $U_2@C_{78}$ and $U_2C@C_{78}$ (see Fig. 5). LDI-TOF monitoring showed the exclusive inclusion of $U_2@C_{78}$. LDI-TOF analysis of the released guest further confirmed the specific molecular recognition of $U_2@C_{78}$ while $U_2C@C_{78}$ remained in the starting sample solution, thus pointing towards the possible separation and purification of C_{78}-based EMF differing only in the internal cluster.

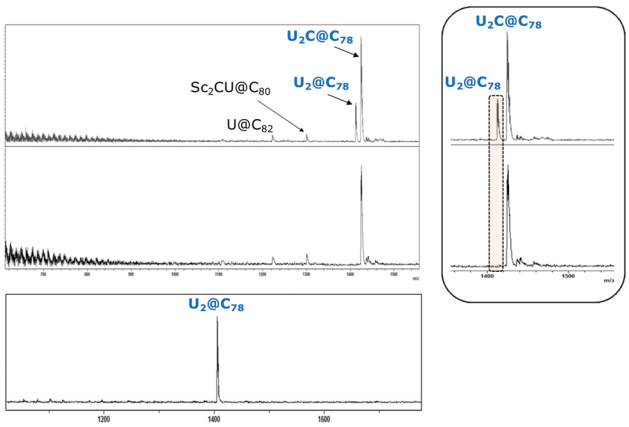

Fig. 5 LDI-TOF monitoring of the remaining supernatant over time during the selective molecular recognition of $U_2@C_{78}$ in front of $U_2C@C_{78}$ (top); spectrum of pure $U_2@C_{78}$ released from $\mathbf{1}\cdot(BArF)_8$ (bottom).

Finally, we attempted the stepwise encapsulation of $U_2@C_{78}$ and $U_2C@C_{78}$ using a complex soot, which included also $U_2@C_{80}$, mono-U-based EMF, Sc_3N-based EMF and empty fullerene cages. On monitoring the composition of the soot by LDI-TOF (Fig. 6), the peak attributed to $U_2@C_{78}$ completely disappeared (after 2 hours) upon the addition of precise amounts of $\mathbf{1}\cdot(BArF)_8$. The nanocapsule was filtered and the guest was liberated, obtaining pure $U_2@C_{78}$ as ascertained by LDI-TOF. Subsequently, additional amounts of fresh crystalline $\mathbf{1}\cdot(BArF)_8$ were added, observing a progressive selective decrease of the $U_2C@C_{78}$ peak. Liberation of the guest allowed the identification of pure $U_2C@C_{78}$.

It is worth noting that the very low concentration of the di-uranium-based C_{78} EMFs present in the soot used makes it very complicated to spectrometrically characterize the host–guest complexes formed during the molecular recognition experiments. Despite these difficulties, the $U_2C@C_{78}\subset\mathbf{1}\cdot(BArF)_8$ complex was identified by ESI-MS (see Fig. S1†).

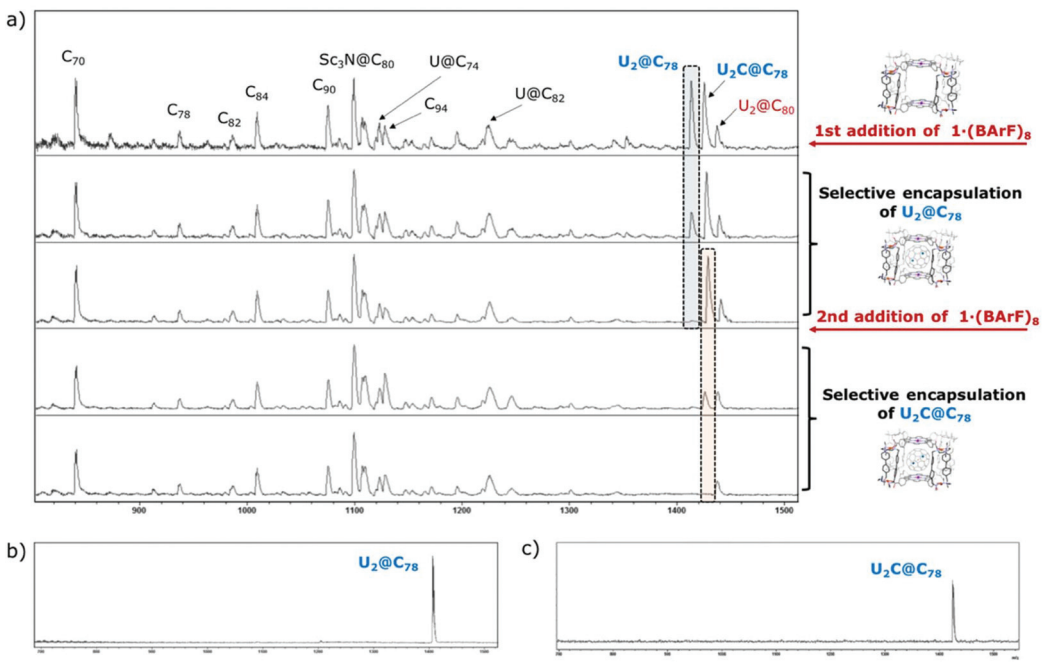

Fig. 6 (a) LDI-TOF monitoring of the remaining supernatant over time during the selective molecular recognition of $U_2@C_{78}$; (b) spectrum of pure $U_2@C_{78}$ and (c) pure $U_2@C_{78}$ released from $\mathbf{1}\cdot(BArF)_8$.

The encapsulation of $Sc_3N@C_{78}$ into **1**·$(BArF)_8$ in front of $Sc_3N@C_{80}$ is thermodynamically and also kinetically preferred, as demonstrated by competition experiments shown in Fig. S3 and S4.†

To gain a deeper understanding of the reasons behind the selectivity of **1**·$(BArF)_8$ for di-uranium@C_{78} EMFs, DFT calculations were performed to compute the binding energies (BEs) between the two porphyrins of the nanocapsule and the EMFs $U_2@I_h$-C_{80} and $U_2@D_{3h}$-C_{78} in a similar manner as previously reported by us.[21] A systematic study has shown that the interaction energy between the porphyrins and the fullerenes changes significantly with the cage orientation with respect to the porphyrins. The position of the uranium ions inside these cages, however, does not affect so much the interaction energies. In particular, for the highly symmetric I_h-C_{80} the two U atoms have free rotation at room temperature. For D_{3h}-C_{78} the U atoms prefer to occupy the positions along the C_3 axis (Fig. 7 top).

The computed BEs between the EMF and the porphyrins for the structures represented in Fig. 7 are compiled in Table 1. These values from our simplified model would indicate that from a thermodynamic point of view the capture of the $U_2@I_h$-C_{80} EMF would be slightly favored, even though the relative binding energies and the porphyrin–porphyrin separations for the lowest energy orientations of the I_h-C_{80} and D_{3h}-C_{78} cages inside the nanocapsule are not that different. However, a more detailed inspection of the computed structures shows that the optimal dispositions of the EMFs display slightly shorter porphyrin–porphyrin separation for $U_2@C_{78}$. The difference is only about 0.2 Å, but it could be significant if we take into account that the empty nanocapsule **1**·$(BArF)_8$ used in the current experiments has a Zn⋯Zn separation of about 12 Å in the previously reported crystal structure,[21] considerably shorter than the equilibrium values computed in our models (Table 1).

To better evaluate the effect of the breathing of the cage, we have explored how the energy changes when the porphyrin–porphyrin distance shrinks from 14 Å to 13 Å. For the energy scan in Fig. 8, the structures of the porphyrins and EMFs remain frozen and only the porphyrin–porphyrin distance changes. The values in Fig. 8 and Table 2 confirm three main points: (1) the optimal Zn–Zn distances are somewhat longer for I_h-C_{80} EMFs, (2) the binding energy between porphyrin and EMF is slightly larger for I_h-C_{80} and (3) as the porphyrin–porphyrin compression progresses the binding energy increases with a lower slope for D_{3h}-C_{78}. Because of the cylindrical shape of the D_{3h}-C_{78} cage, the energy destabilization of the system is smaller for this fullerene. The difference in BEs between structures **2** and **4** is larger than 8 kcal mol^{-1} at a Zn–Zn distance of 13 Å, with the D_{3h}-C_{78} EMF displaying the largest encapsulation energy. Interestingly, if we allow the fullerene to relax its structure, we observe that C_{80} reorients with respect to the porphyrins at 13 Å, and its BE increases from −33.6 to −38.8 kcal mol^{-1}, whereas the reorganization for the D_{3h}-C_{78} cage is somewhat smaller with an energy change of 3.55 kcal mol^{-1}, from −41.1 to −44.6 kcal mol^{-1}. Thus, the binding energy

Table 1 Binding energies between the endohedral fullerene and two porphyrins

	$U_2@D_{3h}$-C_{78}			$U_2@I_h$-C_{80}		
	1	**2**	**3**	**4**	**5**	**6**
BE[a]	−58.5	−56.9	−48.4	−59.1	−58.9	−52.4
d(Zn⋯Zn)[b]	13.68	13.65	14.48	13.80	13.95	14.26

[a] Binding energies computed at the BLYP/TZP(D3) level are given in kcal mol^{-1}. [b] Zn⋯Zn separations are in Å.

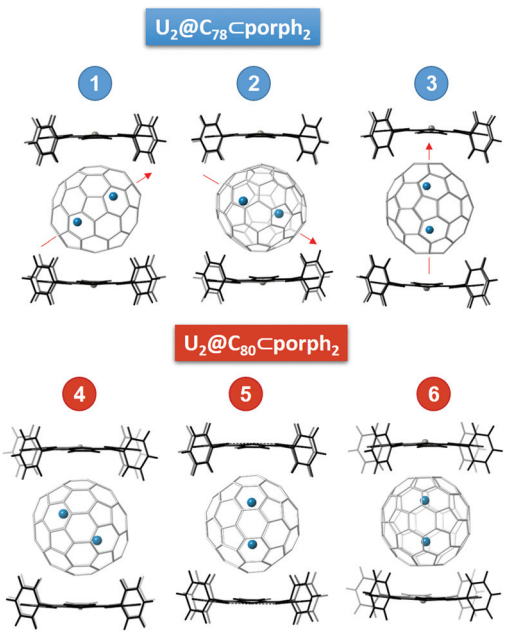

Fig. 7 The lowest energy orientation of $U_2@D_{3h}$-C_{78} (top) and $U_2@I_h$-C_{80} (bottom) in a simplified two tetraphenyl-porphyrin model.

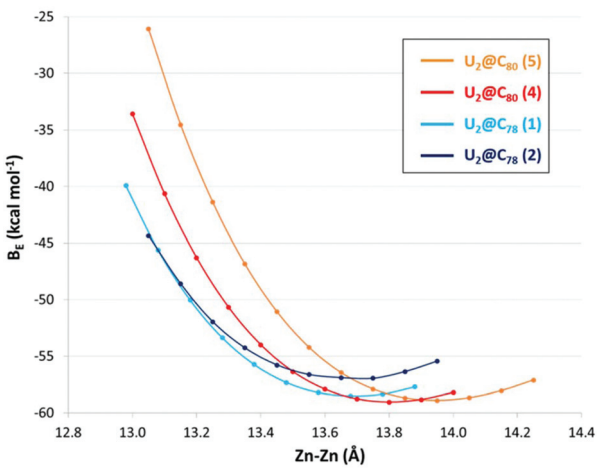

Fig. 8 Energy scan along the Zn⋯Zn separation maintaining porphyrins and fullerenes fixed. The EMF numeration is identical to that in Fig. 7.

Table 2 Binding energies[a] between the endohedral fullerene and two porphyrin models at different Porph···Porph distances

	$U_2@D_{3h}$-C_{78}		$U_2@I_h$-C_{80}	
d(Zn···Zn)[b]	**1**	**2**	**4**	**5**
13.0	−41.1	−41.9	−33.7	−21.5
13.2	−50.6	−50.4	−46.3	−38.1
13.4	−56.0	−55.2	−54.1	−49.1
13.6	−58.2	−57.0	−58.0	−55.5
13.8	−58.1	−56.7	−59.1	−58.4
14.0	−56.6	−55.1	−58.3	−58.8

[a] Binding energies computed at the BLYP/TZP(D3) level are given in kcal mol^{-1}. [b] Zn···Zn separations are in Å.

difference between the two EMFs is still larger than 6 kcal mol^{-1}. These results suggest that the shape of D_{3h}-C_{78} is more suitable than that of I_h-C_{80} for a relatively small nanocapsule like **1**·(BArF)$_8$, or similarly, that the energy penalty for the breathing of the nanocapsule to catch the EMF is smaller for the flattened D_{3h}-C_{78} than for the spherical I_h-C_{80}. This breathing ability is somewhat reminiscent of the one exhibited by some MOFs.[23]

A similar behavior was observed for $U_2C@D_{3h}$-C_{78}. When an extra C is added into the center of the $U_2@C_{78}$ fullerene, affording a linear U_2C cluster as the most stable conformer, the porphyrin–porphyrin separation and the calculated binding energies are exactly the same as those found for $U_2@D_{3h}$-C_{78} (Fig. S5†). Although very recently DFT calculations for several $U_2C@C_{2n}$ endofullerenes including $U_2C@D_{3h}$-C_{78} suggested that the U═C═U cluster takes a bent form inside the D_{3h}-C_{78} cage,[24] we have verified that the linear arrangement is significantly lower in energy (Fig. S6†). The presence of the central carbon atom and the change in the formal oxidation state of uranium ions from +3 to +5 hardly modifies the electron density on the fullerene surface, as suggested by the molecular electrostatic potential distribution maps represented in Fig. 9. Thus, our very simplified model cannot discriminate the different behaviors observed for $U_2C@D_{3h}$-C_{78} and $U_2@D_{3h}$-C_{78} endohedral metallofullerenes, since the uranium carbide is only captured once $U_2@D_{3h}$-C_{78} has been completely removed from the soot (Fig. 5 and 6). This means that more sophisticated models and, probably, molecular dynamics simulations will be needed to better understand the phenomena of encapsulation of fullerenes by nanocapsules like **1**·(BArF)$_8$ or similar ones.

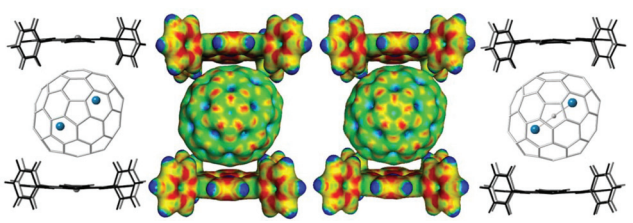

Fig. 9 Comparison of computed structures and molecular electrostatic potential maps for $U_2@D_{3h}$-C_{78}⊂porph$_2$ (left, structure **1** in Fig. 7) and $U_2C@D_{3h}$-C_{78}⊂porph$_2$ in their optimal orientations.

Conclusions

In summary, we report here the ability of supramolecular nanocapsule **1**·(BArF)$_8$ to selectively encapsulate U-based EMFs from highly complex soot containing empty fullerenes and EMFs, ranging from C_{60} to C_{96}. Moreover, the supramolecular host is capable of discriminating C_{78}-based EMFs from C_{80}-based EMFs, thus showing an exquisite ability to discriminate among very similar EMFs. This selectivity stems from the shape differences between a spherical I_h-C_{80} and a flattened D_{3h}-C_{78} carbon cage, and causes an enhanced interaction between the carbon cage and the porphyrin units of the host. Computational analysis also suggests that the breathing ability of the host in the solid state is somewhat limited and that results in a lower breathing energy penalty towards a highly favourable encapsulation of the ellipsoidal D_{3h}-C_{78}-based EMF. Moreover, nanocapsule **1**·(BArF)$_8$ can also sequentially and selectively encapsulate the same D_{3h}-C_{78} carbon cage differing only in the nature of the endohedral cluster, *i.e.* U_2 *vs.* U_2C. This indicates that besides the shape of the carbon cage, the cluster electronics are at interplay in finally determining the affinity for the host. The non-chromatographic supramolecular purification of U-based EMFs reported here has proven to be a viable alternative to HPLC methods, and pure $U_2@D_{3h}$-C_{78} and $U_2C@D_{3h}$-C_{78} EMFs may be accumulated and potentially find utility in several research fields. Moreover, nanocapsule **1**·(BArF)$_8$ and other supramolecular analogues might be designed as platforms to selectively purify targeted EMFs of interest in complex soot.

Conflicts of interest

There are no conflicts to declare.

Acknowledgements

We acknowledge financial support from GenCat (2017 SGR 264 and 2017 SGR 629) and MINECO-Spain (CTQ2016-77989-P and CTQ2017-87269-P). L. E. thanks the US National Science Foundation (NSF) for generous support of this work under the NSF-PREM program (DMR-1205302) and CHE-1408865. The Robert A. Welch Foundation is also gratefully acknowledged for an endowed chair to L. E. (Grant AH-0033). X. R. and J. M. P. are also grateful to ICREA foundation for ICREA-Acadèmia awards.

Notes and references

1 S. Yang, T. Wei and F. Jin, *Chem. Soc. Rev.*, 2017, **46**, 5005–5058.

2 X. Lu, T. Akasaka and S. Nagase, *Chem. Commun.*, 2011, **47**, 5942–5957.
3 X. Zhang, Y. Wang, R. Morales-Martínez, J. Zhong, C. de Graaf, A. Rodríguez-Fortea, J. M. Poblet, L. Echegoyen, L. Feng and N. Chen, *J. Am. Chem. Soc.*, 2018, **140**, 3907–3915.
4 X. Zhang, W. Li, L. Feng, X. Chen, A. Hansen, S. Grimme, S. Fortier, D.-C. Sergentu, T. J. Duignan, J. Autschbach, S. Wang, Y. Wang, G. Velkos, A. A. Popov, N. Aghdassi, S. TDuhm, X. Li, J. Li, L. Echegoyen, W. H. E. Schwarz and N. Chen, *Nat. Commun.*, 2018, **9**, 2753.
5 R. Westerström, J. Dreiser, C. Piamonteze, M. Muntwiler, S. Weyeneth, H. Brune, S. Rusponi, F. Nolting, A. Popov, S. Yang, L. Dunsch and T. Greber, *J. Am. Chem. Soc.*, 2012, **134**, 9840–9843.
6 S. Osuna, M. Swart and M. Solà, *J. Am. Chem. Soc.*, 2009, **131**, 129–139.
7 S. Osuna, M. Swart, J. M. Campanera, J. M. Poblet and M. Solà, *J. Am. Chem. Soc.*, 2008, **130**, 6206–6214.
8 M. Garcia-Borràs, S. Osuna, J. M. Luis, M. Swart and M. Solà, *Chem. – Eur. J.*, 2012, **18**, 7141–7154.
9 N. Martín, *Chem. Commun.*, 2006, 2093–2104, DOI: 10.1039/B601582B.
10 C. M. Cardona, A. Kitaygorodskiy and L. Echegoyen, *J. Am. Chem. Soc.*, 2005, **127**, 10448–10453.
11 Y. Iiduka, O. Ikenaga, A. Sakuraba, T. Wakahara, T. Tsuchiya, Y. Maeda, T. Nakahodo, T. Akasaka, M. Kako, N. Mizorogi and S. Nagase, *J. Am. Chem. Soc.*, 2005, **127**, 9956–9957.
12 H. Shinohara and N. Tagmatarchis, in *Endohedral Metallofullerenes*, Wiley, 2015, pp. 43–68, DOI: 10.1002/9781118698006.ch4.
13 S. Stevenson, K. Harich, H. Yu, R. R. Stephen, D. Heaps, C. Coumbe and J. P. Phillips, *J. Am. Chem. Soc.*, 2006, **128**, 8829–8835.
14 S. Stevenson, M. A. Mackey, J. E. Pickens, M. A. Stuart, B. S. Confait and J. P. Phillips, *Inorg. Chem.*, 2009, **48**, 11685–11690.
15 K. Akiyama, T. Hamano, Y. Nakanishi, E. Takeuchi, S. Noda, Z. Wang, S. Kubuki and H. Shinohara, *J. Am. Chem. Soc.*, 2012, **134**, 9762–9767.
16 M. R. Cerón, F. F. Li and L. Echegoyen, *Chem. – Eur. J.*, 2013, **19**, 7410–7415.
17 L. P. Hernández-Eguía, E. C. Escudero-Adán, J. R. Pinzón, L. Echegoyen and P. Ballester, *J. Org. Chem.*, 2011, **76**, 3258–3265.
18 M.-Y. Ku, S.-J. Huang, S.-L. Huang, Y.-H. Liu, C.-C. Lai, S.-M. Peng and S.-H. Chiu, *Chem. Commun.*, 2014, **50**, 11709–11712.
19 Y. Nakanishi, H. Omachi, S. Matsuura, Y. Miyata, R. Kitaura, Y. Segawa, K. Itami and H. Shinohara, *Angew. Chem., Int. Ed.*, 2014, **53**, 3102–3106.
20 C. Fuertes-Espinosa, C. García-Simón, E. Castro, M. Costas, L. Echegoyen and X. Ribas, *Chem. – Eur. J.*, 2017, **23**, 3553–3557.
21 C. Fuertes-Espinosa, A. Gómez-Torres, R. Morales-Martínez, A. Rodríguez-Fortea, C. García-Simón, F. Gándara, I. Imaz, J. Juanhuix, D. Maspoch, J. M. Poblet, L. Echegoyen and X. Ribas, *Angew. Chem., Int. Ed.*, 2018, **57**, 11294–11299.
22 C. García-Simón, M. Garcia-Borràs, L. Gómez, T. Parella, S. Osuna, J. Juanhuix, I. Imaz, D. Maspoch, M. Costas and X. Ribas, *Nat. Commun.*, 2014, **5**, 5557.
23 A. Schneemann, V. Bon, I. Schwedler, I. Senkovska, S. Kaskel and R. A. Fischer, *Chem. Soc. Rev.*, 2014, **43**, 6062–6096.
24 Y. Li, L. Yang, Z. Li, Q. Hou, L. Li and P. Jin, *Inorg. Chem.*, 2019, **58**, 10648–10655.